RESEARCH ARTICLE

Differential Synaptic Loss in β-Amyloid Positive Versus β-Amyloid Negative Corticobasal Syndrome

Negin Holland, MRCP, PhD,[1,2*] George Savulich, PhD,[3] P. Simon Jones, MSc,[1] David J. Whiteside, MRCP, PhD,[1,2] Duncan Street, MRCP, PhD,[1] Peter Swann, MRCPsych,[3] Michelle Naessens, MSc,[1] Maura Malpetti, PhD,[1] Young T. Hong, PhD,[1,4] Tim D. Fryer, PhD,[1,4] Timothy Rittman, MRCP, PhD,[1] Eoin Mulroy, FRACP,[5] Franklin I. Aigbirhio, DPhil,[1] Kailash P. Bhatia, MD, DM, FRCP,[5] John T. O'Brien, FRCPsych, DM,[2,3] and James B. Rowe, FRCP, PhD[1,2,6]

[1]*Department of Clinical Neurosciences, University of Cambridge, Cambridge Biomedical Campus, Cambridge, United Kingdom*
[2]*Cambridge University Hospitals NHS Foundation Trust, Cambridge, United Kingdom*
[3]*Department of Psychiatry, University of Cambridge, Cambridge Biomedical Campus, Cambridge, United Kingdom*
[4]*Wolfson Brain Imaging Centre, University of Cambridge, Cambridge, United Kingdom*
[5]*Department of Clinical and Movement Neurosciences, UCL Queen Square Institute of Neurology, London, United Kingdom*
[6]*Medical Research Council Cognition and Brain Sciences Unit, University of Cambridge, Cambridge, United Kingdom*

ABSTRACT: Background/Objective: The corticobasal syndrome (CBS) is a complex asymmetric movement disorder, with cognitive impairment. Although commonly associated with the primary 4-repeat-tauopathy of corticobasal degeneration, clinicopathological correlation is poor, and a significant proportion is due to Alzheimer's disease (AD). Synaptic loss is a pathological feature of many clinical and preclinical tauopathies. We therefore measured the degree of synaptic loss in patients with CBS and tested whether synaptic loss differed according to β-amyloid status.

Methods: Twenty-five people with CBS, and 32 age-/sex-/education-matched healthy controls participated. Regional synaptic density was estimated by [^{11}C]UCB-J non-displaceable binding potential (BP_{ND}), AD-tau pathology by [^{18}F]AV-1451 BP_{ND}, and gray matter volume by T1-weighted magnetic resonance imaging. Participants with CBS had β-amyloid imaging with ^{11}C-labeled Pittsburgh Compound-B ([^{11}C]PiB) positron emission tomography. Symptom severity was assessed with the progressive supranuclear palsy-rating-scale, the cortical basal ganglia functional scale, and the revised Addenbrooke's Cognitive Examination. Regional differences in BP_{ND} and gray matter volume between groups were assessed by ANOVA.

Results: Compared to controls, patients with CBS had higher [^{18}F]AV-1451 uptake, gray matter volume loss, and reduced synaptic density. Synaptic loss was more severe and widespread in the β-amyloid negative group. Asymmetry of synaptic loss was in line with the clinically most affected side.

Discussion: Distinct patterns of [^{11}C]UCB-J and [^{18}F]AV-1451 binding and gray matter volume loss, indicate differences in the pathogenic mechanisms of CBS according to whether it is associated with the presence of Alzheimer's disease or not. This highlights the potential for different therapeutic strategies in CBSs. © 2024 The Authors. *Movement Disorders* published by Wiley Periodicals LLC on behalf of International Parkinson and Movement Disorder Society.

Key Words: Alzheimer's disease; CBD/PSP; corticobasal syndrome; synaptic loss; β-amyloid status

***Correspondence to:** Dr. Negin Holland, University of Cambridge, Herschel Smith Building, Robinson Way, Cambridge Biomedical Campus, Cambridge, CB2 0SZ, UK; E-mail: nda26@cam.ac.uk

John T. O'Brien and James B. Rowe joint senior authors.

Relevant conflicts of interest/financial disclosures: The authors do not have any competing interest pertaining to this manuscript.

Funding agencies: The study was supported by the Wellcome Trust (220258), the Cambridge Centre for Parkinson-Plus (RG95450); the National Institute for Health and Care Research (NIHR) Cambridge Biomedical Research Centre (NIHR203312); Medical Research Council (MC_UU_00030/14; MR/T033371/1); Dementias Platform United Kingdom (UK) (RG94383; and G103658); Association of British Neurologists, Patrick Berthoud Charitable Trust (RG99368), and Race Against Dementia Alzheimer's Research UK (ARUK-RADF2021A-010). The views expressed are those of the authors and not necessarily those of the NIHR or the Department of Health and Social Care. For the purpose of open access, the author has applied a CCBY public copyright license to any author accepted manuscript version arising from this submission.

Received: 8 January 2024; **Revised:** 12 March 2024; **Accepted:** 29 March 2024

Published online in Wiley Online Library (wileyonlinelibrary.com). DOI: 10.1002/mds.29814

The corticobasal syndrome (CBS) is a highly heterogeneous neurodegenerative disorder.[1] It is characterized by the combination of a movement disorder (akinetic-rigidity, dystonia, myoclonus, alien-limb, or apraxia) with cognitive decline (affecting language, visuospatial, executive function and memory domains).[2,3] At post mortem, CBS is often associated with the 4-repeat (4R) tauopathy of corticobasal degeneration (CBD), with some cases of the closely related tauopathy of progressive supranuclear palsy (PSP). However, the pathological correlation with clinical diagnostic criteria is poor,[2,4-6] and pathologies other than CBD and PSP account for 30% to 50% of cases; the most frequent alternative pathology being Alzheimer's disease (AD).[1,7] Such pathophysiological heterogeneity presents not only a clinical diagnostic challenge, but also an obstacle to rational mechanisms-based therapeutic strategies and clinical trials design.

Here, we focus on the difference between AD and non-AD causes of CBS, where the non-AD causes are most likely to be CBD (or PSP). They differ in their associated molecular pathologies (4R tau in CBD/PSP vs. 3R/4R tau with β-amyloid pathology in AD), and biomarkers in blood,[8] cerebrospinal fluid,[9] and neuroimaging.[10] Fluorodeoxyglucose positron emission tomography (PET) imaging differs between β-amyloid-positive and β-amyloid-negative patients.[11-15] Magnetic resonance imaging (MRI) shows asymmetric cortical and subcortical gray and white matter changes, but the ability of structural MRI to differentiate the molecular pathology of CBS are limited.[16]

Synaptic loss is common in preclinical models and neuropathological studies of diverse neurodegenerative diseases, including multiple tauopathies. It is a convergence point for the neurotoxicity of misfolded protein aggregation, mitochondrial stress, and neuroinflammation and occurs before neurodegeneration in transgenic tauopathies.[17] The radioligand [^{11}C]UCB-J can be used to estimate synaptic density in vivo, based on its affinity for the presynaptic vesicle glycoprotein SV2A.[18] This ligand reveals significant synaptic loss in AD,[19,20] frontotemporal dementia,[21,22] Lewy body dementia,[23,24] Parkinson's disease,[25] and PSP.[26] The synaptic loss correlates with clinical disease severity and is more closely correlated with severity than the level of β-amyloid, tau or atrophy, in AD,[27] PSP,[28] and frontotemporal dementia.[22]

The aim of this study was to examine the heterogeneity of CBS in terms of synaptic density, as measured by [^{11}C]UCB-J PET, compared to [^{18}F]AV-1451 uptake and gray matter volume loss. Our principal hypotheses were that: (1) the extent and severity of synaptic loss differs according to β-amyloid status; and (2) the spatial distribution of synaptic loss correlates with the patients' clinically most affected side. Secondary hypotheses were that (3) [^{18}F]AV-1451 uptake and volume loss differ according to β-amyloid status.

Methods

Participants

Twenty-five people with possible or probable CBS, according to the Armstrong criteria,[2] were recruited from regional specialist clinics at the Cambridge University Centre for Parkinson-plus, and National Hospital for Neurology and Neurosurgery, London. Thirty-two healthy volunteers were recruited from the National Institute for Health Research Join Dementia Research register. Participants were screened using the inclusion/exclusion criteria set out in Holland et al (2020)[26] All participants undertook synaptic imaging with [^{11}C]UCB-J PET, and tau imaging with [^{18}F]AV-1451 (flortaucipir) PET. Participants with CBS had amyloid PET imaging using 11C-labeled Pittsburgh Compound B ([^{11}C]PiB).

Participants undertook the revised Addenbrooke's Cognitive Examination-Revised (ACE-R) and Mini-Mental State Examination (MMSE); disease severity was measured with the PSP rating scale (aimed at diseases caused by 4R tauopathies),[29] and the Cortical Basal ganglia Functional Scale (CBFS).[30] The most clinically affected body side (as per patient reported symptoms or clinician review) were recorded. Functional disease severity was rated by the Cambridge Behavioral Inventory (CBI), and the Clinical Dementia Rating Scale sum-of-boxes (CDR).

Standard Protocol Approvals, Registrations, and Patient Consents

The study was approved by the Cambridge Research Ethics Committee (18/EE/0059) and the United Kingdom Administration of Radioactive Substances Advisory Committee. Participants provided written informed consent in accordance with the Declaration of Helsinki.

Neuroimaging

[^{11}C]UCB-J PET and Gray Matter Volume (MRI)

The procedure for [^{11}C]UCB-J synthesis, dynamic PET data acquisition, image reconstruction and kinetic analysis are reported in detail in Holland et al (2020)[26] In brief, dynamic PET data acquisition was performed on a GE SIGNA PET/MR (GE Healthcare, Waukesha, WI) for 90 minutes immediately after injection, with attenuation correction using a multi-subject atlas method.[31] Emission images were aligned using SPM12 (www.fil.ion.ucl.ac.uk/spm/software/spm12/), and rigidly registered to a T1-weighted MRI acquired during PET data acquisition (repetition time [TR] = 3.6 ms, echo time [TE] = 9.2 ms, 192 sagittal slices, in plane resolution 0.55 × 0.55 mm, interpolated to 1.0 × 1.0 mm; slice thickness, 1.0 mm). For regional analysis, we used a modified version of the n30r83 Hammersmith atlas (http://brain-development.org) including segmentation of brainstem and cerebellar structures, with the atlas non-rigidly registered to the

T1-weighted MRI of each participant, using the Advanced Normalization Tools (ANTs) software.[32] Gray matter volumes were extracted using SPM12 segmentation, for all 95 Hammersmith atlas regions, with 78 brain regions (excluding the ventricles and the corpus callosum) taken forward to regional analysis. Detailed results for all 78 regions are given in Supplementary Tables S1 and S2, Figure 2, and Supplementary Figure S2. Aggregate regional results (frontal lobe, parietal lobe, temporal lobe, occipital lobe, and central structures) are presented in the main manuscript tables for ease of presentation (Table 2).

Correction for partial volume error from cerebrospinal fluid (CSF)[33] was applied to each dynamic PET image and regional time-activity curves extracted. This corrects for the potential presence of CSF in some of the image volumes, which a priori has no synapses. To assess the impact of partial volume correction, time-activity curves were also extracted from the same regions of interest without the application of partial volume correction (discussed in the Supporting Data as "without partial volume correction").

To quantify synaptic density, [^{11}C]UCB-J non-displaceable binding potential (BP_{ND}) was determined using a basis function implementation of the simplified reference tissue model,[34] with the reference tissue defined in the centrum semiovale.[35,36]

[^{18}F]Av-1451 Pet

Dynamic [^{18}F]AV-1451 PET imaging was performed on a GE SIGNA PET/MR for 90 minutes after [^{18}F]AV-1451 injection. [^{18}F]AV-1451 BP_{ND} was determined using a basis function implementation of the simplified reference tissue model,[37] with the reference tissue defined in the inferior cerebellar gray matter,[38] using a 90% threshold on the gray matter probability map, produced by SPM12 smoothed to PET resolution. We acknowledge that [^{18}F]AV-1451 has high affinity for AD-related tau, and low affinity for the 4R-tau of CBD.[39]

[^{11}C]PiB PET

β-Amyloid imaging using [^{11}C]PiB followed Holland et al (2020).[26] [^{11}C]PiB cortical standardized uptake value ratio (SUVR) (50–70 minute post injection) was calculated using the whole cerebellum reference tissue as per the Centiloid project methodology.[40] A negative amyloid status was characterized by a cortical [^{11}C]PiB SUVR <1.21 obtained by converting the Centiloid cut-off of 19 to SUVR using the Centiloid-to-SUVR transformation in Jack et al.[41] Patients with an SUVR >1.21 are referred to as "CBS/Aβ+ve" and those with SUVR <1.21, "CBS/Aβ−ve."

All [^{11}C]UCB-J PET and T1 MRI occurred contemporaneously. [^{18}F]AV-1451 and [^{11}C]PiB PET imaging occurred close to [^{11}C]UCB-J PET (AV-1451: median −3 months; PiB: median + 2 months).

Statistical Analyses

All statistical analyses were implemented in R (version 4.2.0). We compared demographic and clinical variables between patients and controls, using analysis of variance (ANOVA) or χ^2-tests as appropriate.

Linear regression models were used to test for the effect of [^{11}C]UCB-J and [^{18}F]AV-1451 binding, and gray matter volume on disease severity rating scales (PSPRS, CBFS, and ACE-R), allowing for an interaction with brain region, with age as a covariate.

Assessing asymmetry in [^{11}C]UCB-J and [^{18}F]AV-1451BP_{ND} and gray matter volume. The laterality index for synaptic density, from regional [^{11}C]UCB-J BP_{ND} values, was calculated as follows,[42] and correlated with laterality of clinical symptoms:

$$\text{Laterality index(LI)} = \left(\text{Left UCB} - \text{J BP}_{\text{ND}} - \text{Right UCB} - \text{J BP}_{\text{ND}}\right) / \left(\text{Left UCB} - \text{J BP}_{\text{ND}} + \text{Right UCB} - \text{J BP}_{\text{ND}}\right)$$

The laterality index ranges from −1 to +1, indicating left and right dominant synaptic loss on [^{11}C]UCB-J PET, respectively, with 0 indicating symmetry (Fig. 1). We performed a two-way paired-sample ANOVA to test for a difference in [^{11}C]UCB-J BP_{ND} in left versus right brain regions (using 11 aggregate brain regions—frontal, temporal, parietal, occipital lobes, cingulate cortex, and central structures). A post hoc analysis tested for region-by-side interactions (Bonferroni corrected for multiple comparisons, $\alpha = 0.0045$). A binomial logistic regression tested the relationship between the most affected side on clinical examination versus that on [^{11}C]UCB-J PET.

The laterality index for [^{18}F]AV-1451 uptake and gray matter volume followed the same steps as for [^{11}C]UCB-J above.

Differences in [^{18}F]AV-145 binding, [^{11}C]UCB-J Binding, and gray matter volume between patients and controls, and within patients based on β-amyloid status. We compared regional [^{11}C]UCB-J and [^{18}F]AV-1451 BP_{ND}, and gray matter volume between patients and controls, and within the patient cohort (CBS/Aβ+ve versus CBS/Aβ−ve); we used analysis of covariance with age as covariate (and total intracranial volume in the case of gray matter volume comparison). Statistical inferences were corrected for multiple comparisons (Tukey's honestly significant difference [HSD] method), and the resultant *t*-statistics projected onto brain maps with the following contrasts: control > CBS/Aβ+ve, control > CBS/Aβ−ve, CBS/Aβ+ve > CBS/Aβ−ve. Regional [^{11}C]UCB-J and [^{18}F]AV-1451 BP_{ND}, and gray

matter volumes were standardized against the control data; the resulting z-scores were used to calculate effect sizes (Cohen's *d*) for group comparisons.

Given the small numbers of people with CBS in our study, we corroborated our frequentist statistics, with a Bayesian analysis using the software JASP.[43] For each of the abovementioned group comparisons, we report the Bayes factor (BF10) for the alternative hypothesis (that there is a group difference) over the null hypothesis (that there is no group difference) with the following BF interpretations: >100 = extreme, >30 = very strong, >10 = strong, >3 = moderate, and 1–3 = anecdotal evidence for the alternative hypothesis; 0.33–1 = anecdotal, <0.33 = moderate, <0.10 = strong, <0.03 = very strong, <0.01 = extreme evidence for the null hypothesis (Supplementary Tables S3A, B).[44]

Results

Demographics and Clinical Characteristics

Patients and controls were matched in age, sex, and education. Impairments were seen across multiple cognitive domains of the ACE-R and MMSE. There were high endorsements on the CBI, and high scores on the CDR sum-of-boxes. Seventeen of 25 participants with CBS were β-amyloid-negative (CBS/Aβ−ve: SUVR <1.21), and eight positive (CBS/Aβ+ve).

The cognitive screening test performance, symptom severity and duration, and carer burden questionnaires were similar between CBS/Aβ−ve and CBS/Aβ+ve subgroups. Specifically, there were no differences in symptom duration or severity on the PSP/CBFS rating scales. Similar scores were seen on tests of cognition and carer endorsements (Table 1) ($P > 0.05$ and BF10 <1 in support of the null hypothesis). The clinically most affected side was on the right for 10 patients and on the left for 14 patients. One patient had presented with asymmetric symptoms, but was clinically symmetrical by the time of PET imaging and was excluded from the asymmetry analysis.

Relationship between Imaging Parameters and Clinical Severity Scales

Across all patients, higher scores on the PSP rating scale were associated with lower [^{11}C]UCB-J binding

TABLE 1 *Demographics and clinical summary.*

	Control	CBS-All	CBS/Aβ+ve	CBS/Aβ−ve	*P*-value (+ve vs. −ve)	BF_{10} (+ve vs. −ve)
No.	32	25	8	17	–	–
M:F	21:11	13:12	4:4	9:8	ns[a]	–
Age at scan (y)	69.0 (8.6)	70.4 (7.3)	71.3 (7.5)	69.3 (6.9)	ns	0.45
Education (y)	14.2 (3.5)	13.1 (3.0)	14.4 (3.8)	12.5 (2.5)	ns	0.86
Symptom duration at scan (y)	–	5.4 (2.8)	6.2 (2.7)	5.1 (2.9)	ns	0.51
Most affected side (right:left)	–	10:14	1:6	9:8	ns[a]	0.51
Total MMSE (max 30)	29.5 (1.1)	24.2 (6.1)	23.1 (8.2)	25.4 (4.5)	ns	0.41
Total ACE-R (max 100)	96.3 (2.7)	74.8 (20.9)	73.4 (30.1)	76.8 (15.4)	ns	0.56
Attention and orientation (max 18)	17.9 (0.3)	15.4 (3.3)	14.8 (4.6)	16.1 (2.2)	ns	0.45
Fluency (max 14)	12.4 (1.5)	7.4 (3.7)	8.6 (4.5)	6.9 (3.5)	ns	0.58
Language (max 26)	25.7 (0.8)	21.1 (6.9)	21.2 (8.6)	21.6 (6.0)	ns	0.39
Memory (max 26)	24.6 (1.9)	19.8 (6.1)	18.8 (8.7)	20.5 (4.7)	ns	0.50
Visuospatial (max 16)	15.7 (0.6)	11.0 (4.7)	10.0 (5.6)	11.8 (4.4)	ns	0.39
Total PSPRS	–	27.9 (11.4)	28.1 (10.9)	27.1 (11.8)	ns	0.65
Total CBFRS	–	31.7 (16.7)	37.9 (23.7)	29.0 (12.6)	ns	0.57
Total CBI	–	41.7 (25.7)	49.7 (38.7)	40.3 (19.5)	ns	0.51
Total CDR	–	8.4 (6.4)	10.4 (9.6)	7.4 (5.0)	ns	0.45

Note: The results are given as mean (standard deviation). Within patient comparisons (+ve vs. −ve) are derived from ANOVA (or [a]χ^2-tests where required). BF_{10} of <1 indicate "anecdotal" evidence for no difference between groups.

Abbreviations: CBS, corticobasal syndrome (Armstrong criteria); CBS/Aβ+ve, β-amyloid positive; CBS/Aβ−ve, β-amyloid negative; BF, Bayes factor 10; M, male; F, female; ns, not significant; MMSE, mini-mental state examination; max, maximum; ACE-R, revised Addenbrooke's cognitive examination; PSPRS, Progressive Supranuclear Palsy Rating Scale CBFRS, cortical basal ganglia functional scale; CBI, revised Cambridge Behavioural Inventory; CDR, clinical dementia rating scale; ANOVA, analysis of variance.

($\beta = -3.0$, F(p) = 14.1 [<0.01]), and higher [^{18}F]AV-1451 binding ($\beta = 1.1$, F(p) = 12.8 [0.03]), but not associated with gray matter volume loss or age. Similarly, higher scores on the CBFS, were associated with lower [^{11}C]UCB-J binding ($\beta = -18.7$, F(p) = 8.7 [<0.01]), particularly within the bilateral parietal lobes, bilateral middle, and inferior frontal gyri, right precentral gyrus and right posterior temporal lobe. Higher CBFS scores were associated with higher [^{18}F]AV-1451 binding ($\beta = 27.9$, F(p) = 98.9 [<0.001]), and age ($\beta = 0.15$, F(p) = 7.8 [<0.01]). Better performance on the ACE-R was associated with higher [^{11}C]UCB-J binding ($\beta = 6.7$ F(p) = 51.1 [<0.001]), higher gray matter volume ($\beta = 0.1$ F(p) = 64.4 [<0.001]), younger age ($\beta = -0.12$, F(p) = 36.0 [<0.001]), and lower [^{18}F]AV-1451 binding ($\beta = -36.7$, F(p) = 160.3 [<0.001]).

Asymmetric [^{11}C]UCB-J and [^{18}F]AV-1451 Binding and Gray Matter Atrophy

Across all CBS patients, there was asymmetric [^{11}C]UCB-J and [^{18}F]AV-1451 binding and gray matter atrophy. [^{11}C]UCB-J BP_{ND} was asymmetric within the following brain regions: frontal and occipital lobes ($P = 0.01$), cingulate ($P < 0.0001$), insula ($P < 0.0001$), thalamus ($P = 0.01$), caudate nucleus ($P < 0.0001$), pallidum ($P < 0.0001$), and the putamen ($P = 0.03$), with the pallidum, caudate nucleus, cingulate, and insula significant after correction for multiple comparisons. The most affected side on [^{11}C]UCB-J imaging, correlated with clinical severity in the contralateral body part (logistic regression: $\beta = -1.4$, $P < 0.0001$), and in the case of asymmetry in the cerebellum only, with the ipsilateral body part (logistic regression: $\beta = 3.4$, $P < 0.006$) (Fig. 1 and Supplementary Fig. S1).

[^{18}F]AV-1451 BP_{ND} was asymmetric within the frontal ($P = 0.03$) and the parietal lobe ($P = 0.04$), uncorrected. The side affected most on imaging was not associated with clinical severity in the contralateral body part. Gray matter atrophy (adjusted for total intracranial volume) was asymmetric within the following brain regions: frontal lobe ($P < 0.001$), temporal ($P < 0.001$), parietal lobe ($P < 0.01$), cingulate ($P < 0.001$), insula ($P < 0.001$), putamen ($P < 0.01$), and thalamus ($P < 0.01$), with all but the parietal lobe and the putamen significant after correction for multiple comparison. Asymmetry on atrophy was not significantly associated with asymmetry on clinical assessment.

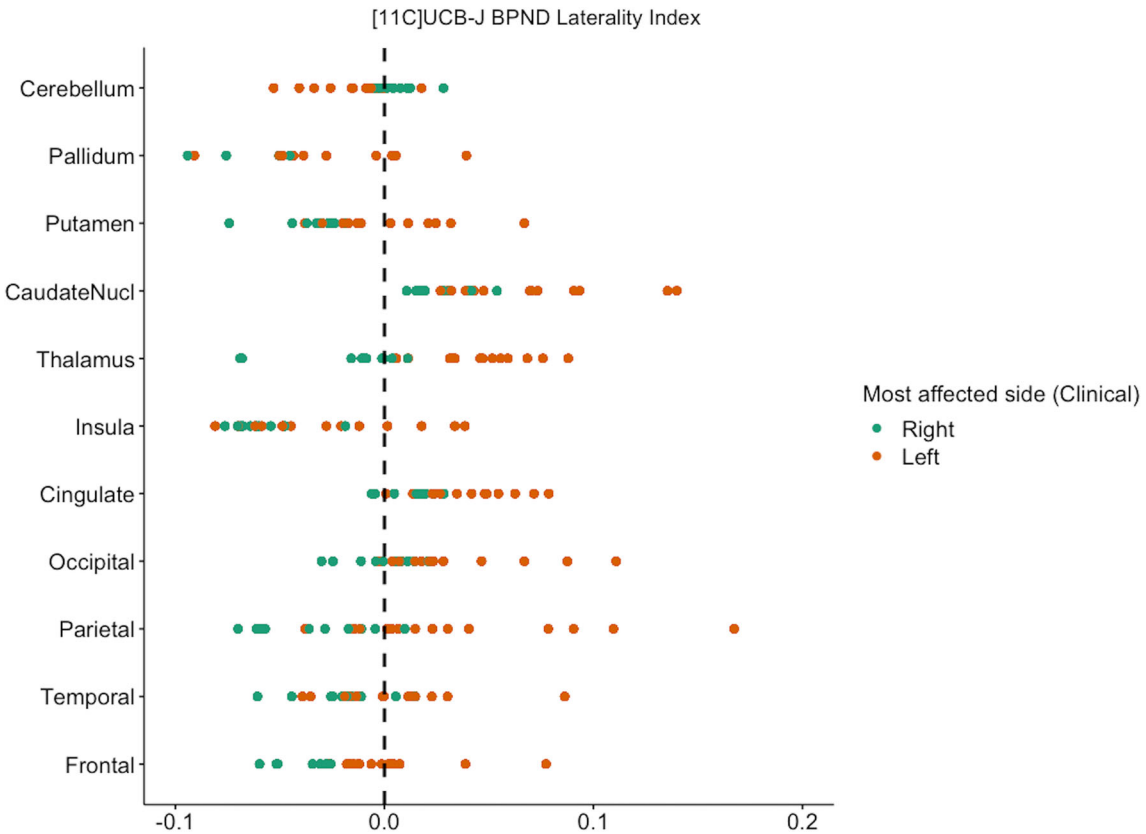

FIG. 1. Laterality index for [^{11}C]UCB-J non-displaceable binding potential (BP_{ND}) (partial volume corrected) in aggregate brain regions. Negative values denote left-sided and positive values right-sided predominant synaptic loss on PET imaging. Results are color coded by the patient's clinically most affected side. For those participants with predominantly left-sided symptoms (red), synaptic loss was more severe on the right (and ipsilateral cerebellum), and vice versa for those with right-sided predominant symptoms (green).

TABLE 2 t *Values, effect sizes (Cohen's* d*), and* P *values (Tukey's HSD corrected for multiple comparison) for [*^{18}*F]AV-1451* BP_{ND} *and [*^{11}*C]UCB-J* BP_{ND} *(both with partial volume correction), and GM volume comparisons in aggregate brain regions, between (A) healthy controls and CBS/Aβ+ve (control > CBS/Aβ+ve), (B) healthy controls and CBS/Aβ−ve (control > CBS/Aβ−ve), and (C) CBS/Aβ+ve and CBS/Aβ−ve (CBS/Aβ+ve > CBS/Aβ−ve)*

	[^{18}F]AV-1451			[^{11}C]UCB-J			GM volume		
	***t* value**	**Cohen's *d***	***P* value**	***t* value**	**Cohen's *d***	***P* value**	***t* value**	**Cohen's *d***	***P* value**
(A) Control > CBS/Aβ+ve									
Region									
Frontal_l	−3.06	−1.23	0.01	1.04	0.37	ns	3.36	1.21	0.00
Frontal_r	−3.84	−1.30	0.00	2.07	0.76	ns	4.18	1.61	0.00
Temporal_l	−3.82	−1.21	0.00	1.15	0.34	ns	3.56	1.44	0.00
Temporal_r	−4.03	−1.17	0.00	2.14	0.65	ns	4.19	1.69	0.00
Parietal_l	−3.73	−1.12	0.00	3.16	1.10	0.01	4.29	1.74	0.00
Parietal_r	−4.10	−1.18	0.00	4.96	1.91	0.00	4.94	2.26	0.00
Occipital_l	−3.37	−1.00	0.00	1.97	0.59	ns	2.87	1.23	0.02
Occipital_r	−4.19	−1.17	0.00	3.15	1.06	0.01	3.86	1.83	0.00
Insula_l	−2.60	−0.99	0.03	0.31	0.02	ns	1.63	0.35	ns
Insula_r	−2.99	−0.98	0.01	1.94	0.56	ns	2.72	0.92	0.02
Cingulate_l	−3.78	−1.17	0.00	0.93	0.26	ns	3.20	1.15	0.01
Cingulate_r	−4.24	−1.22	0.00	1.64	0.51	ns	2.69	1.21	0.03
Thalamus_l	0.00	0.00	ns	1.07	0.38	ns	3.58	1.63	0.00
Thalamus_r	−0.60	−0.37	ns	2.28	0.85	ns	3.99	2.26	0.00
CaudateNucl_l	0.27	0.13	ns	1.49	0.39	ns	5.17	1.80	0.00
CaudateNucl_r	0.19	0.08	ns	1.93	0.56	ns	6.49	2.06	0.00
Putamen_l	−1.82	−0.96	ns	1.15	0.30	ns	2.26	0.78	ns
Putamen_r	−2.91	−1.37	0.02	1.59	0.47	ns	2.73	1.24	0.02
Pallidum_l	−0.41	−0.27	ns	0.38	0.04	ns	0.54	−0.02	ns
Pallidum_r	−1.17	−0.57	ns	1.94	0.48	ns	−0.20	−0.44	ns
Brainstem_mid	0.59	0.49	ns	−0.26	−0.39	ns	0.07	−0.10	ns
Brainstem_pon	0.67	0.47	ns	−0.04	−0.15	ns	−2.31	−0.68	ns
Cerebellum_l	−1.17	−0.94	ns	0.32	0.17	ns	2.23	0.84	ns
Cerebellum_r	−1.22	−0.68	ns	−0.17	−0.01	ns	2.02	0.71	ns
(B) Control > CBS/Aβ−ve									
Region									
Frontal_l	−0.92	−0.32	ns	4.69	1.55	0.00	3.88	1.40	0.00
Frontal_r	−0.70	−0.27	ns	4.44	1.34	0.00	4.09	1.39	0.00
Temporal_l	−0.19	−0.08	ns	3.02	1.16	0.01	2.84	1.06	0.02
Temporal_r	−0.06	−0.03	ns	3.30	1.20	0.00	2.79	1.02	0.02
Parietal_l	−0.43	−0.19	ns	4.51	1.51	0.00	3.80	1.34	0.00
Parietal_r	−0.55	−0.27	ns	4.18	1.28	0.00	3.30	1.10	0.00
Occipital_l	0.02	0.01	ns	3.33	1.09	0.00	2.61	0.96	0.03
Occipital_r	−0.29	−0.15	ns	3.62	1.17	0.00	3.05	1.12	0.01

(Continues)

TABLE 2 *Continued*

	[^{18}F]AV-1451			[^{11}C]UCB-J			GM volume		
	***t* value**	**Cohen's *d***	***P* value**	***t* value**	**Cohen's *d***	***P* value**	***t* value**	**Cohen's *d***	***P* value**
Insula_l	−0.64	−0.23	ns	3.72	1.36	0.00	2.00	0.74	ns
Insula_r	0.04	0.02	ns	4.02	1.36	0.00	2.35	1.00	ns
Cingulate_l	−0.03	−0.01	ns	3.84	1.35	0.00	1.49	0.42	ns
Cingulate_r	−0.52	−0.26	ns	3.48	1.19	0.00	0.53	0.08	ns
Thalamus_l	−2.12	−0.64	ns	4.57	1.39	0.00	3.94	1.36	0.00
Thalamus_r	−1.83	−0.55	ns	4.54	1.39	0.00	2.56	0.97	0.04
CaudateNucl_l	0.66	0.21	ns	4.50	2.09	0.00	4.93	1.62	0.00
CaudateNucl_r	0.67	0.23	ns	4.36	1.91	0.00	4.32	1.71	0.00
Putamen_l	−1.53	−0.49	ns	4.51	1.53	0.00	4.17	1.21	0.00
Putamen_r	−1.43	−0.47	ns	4.29	1.42	0.00	4.13	1.14	0.00
Pallidum_l	−2.82	−0.84	0.02	2.82	1.01	0.02	1.22	0.39	ns
Pallidum_r	−2.36	−0.76	ns	3.03	1.13	0.01	1.39	0.59	ns
Brainstem_mid	−2.45	−0.71	0.05	3.06	0.85	0.01	0.11	0.22	ns
Brainstem_pon	−0.75	−0.22	ns	3.60	1.05	0.00	−1.18	−0.23	ns
Cerebellum_l	−1.99	−0.58	ns	4.23	1.37	0.00	2.69	0.81	0.03
Cerebellum_r	−1.59	−0.49	ns	4.21	1.29	0.00	2.86	0.85	0.02
(C) CBS/Aβ+ve > CBS/Aβ−ve									
Frontal_l	2.18	0.75	ns	2.33	0.71	ns	−0.38	−0.23	ns
Frontal_r	3.09	0.97	0.01	1.20	0.34	ns	−0.99	−0.49	ns
Temporal_l	3.43	1.04	0.00	1.05	0.26	ns	−1.29	−0.66	ns
Temporal_r	3.74	1.08	0.00	0.34	0.04	ns	−1.91	−0.73	ns
Parietal_l	3.18	0.95	0.01	0.24	−0.17	ns	−1.30	−0.66	ns
Parietal_r	3.44	0.98	0.00	−1.64	−0.77	ns	−2.25	−1.11	ns
Occipital_l	3.17	0.98	0.01	0.51	0.14	ns	−0.82	−0.36	ns
Occipital_r	3.72	1.04	0.00	−0.37	−0.15	ns	−1.42	−0.64	ns
Insula_l	1.96	0.68	ns	2.32	0.71	ns	−0.10	0.15	ns
Insula_r	2.84	0.89	0.02	1.02	0.32	ns	−0.86	−0.26	ns
Cingulate_l	3.52	1.09	0.00	1.83	0.48	ns	−1.91	−0.69	ns
Cingulate_r	3.59	1.04	0.00	0.92	0.22	ns	−2.10	−1.09	ns
Thalamus_l	−1.57	−0.67	ns	2.21	0.72	ns	−0.54	−0.41	ns
Thalamus_r	−0.79	−0.32	ns	1.07	0.39	ns	−1.89	−1.17	ns
CaudateNucl_l	0.23	0.09	ns	1.78	0.63	ns	−1.32	−0.55	ns
CaudateNucl_r	0.31	0.13	ns	1.28	0.47	ns	−2.95	−1.05	0.01
Putamen_l	0.57	0.26	ns	2.10	0.73	ns	0.84	0.51	ns
Putamen_r	1.67	0.74	ns	1.54	0.57	ns	0.37	0.11	ns
Pallidum_l	−1.70	−0.70	ns	1.62	0.84	ns	0.36	0.41	ns
Pallidum_r	−0.65	−0.25	ns	0.33	0.38	ns	1.16	0.90	ns

(Continues)

TABLE 2 *Continued*

	[^{18}F]AV-1451			[^{11}C]UCB-J			GM volume		
	t value	Cohen's *d*	*P* value	*t* value	Cohen's *d*	*P* value	*t* value	Cohen's *d*	*P* value
Midbrain	−2.36	−0.94	ns	2.38	0.97	ns	0.02	0.30	ns
Pons	−1.19	−0.50	ns	2.56	0.87	0.03	1.31	0.48	ns
Cerebellum_l	−0.37	−0.15	ns	2.66	0.83	0.03	−0.17	0.02	ns
Cerebellum_r	−0.03	−0.01	ns	3.10	0.94	0.01	0.15	0.15	ns

Abbreviations: HSD, honestly significant difference; GM, gray matter; BP_{ND}, non-displaceable binding potential; CBS, corticobasal syndrome; CBS amyloid positive, CBS/Aβ +ve; CBS amyloid negative, CBS/Aβ−ve; ns, not significant.

Differences in [^{18}F]AV-1451 and [^{11}C]UCB-J Binding, and Gray Matter Volume between Patients and Controls, and within Patients Based on β-Amyloid Status

Table 2 (aggregate regions; partial volume corrected), and detailed Supplementary Tables S1A–C (partial volume corrected) and S2A–C (without partial volume correction) summaries the *t* values, Cohen's *d* effect sizes and *P*-values for the regional comparisons in [^{18}F]AV-1451 and [^{11}C]UCB-J BP_{ND}, and gray matter volume, between patients and controls, and within patients. For detailed visualization, the *t* values from the 78 brains regions in Supplementary Tables S1A–C and S2A–C (thresholded at adjusted $P < 0.05$), are illustrated on brain maps in Figure 2A (partial volume corrected), and Supplementary Figure S2A (partial volume uncorrected). In both figures, higher *t*-values depict higher [^{18}F]AV-1451 binding, higher [^{11}C]UCB-J binding, and higher gray matter volume.

Controls > CBS/Aβ+Ve

Frequentist Approach. Compared to controls, the CBS/Aβ+ve group had increased [^{18}F]AV-1451 binding in 51 (of 78) frontal, temporal, parietal, and occipital subregions, in addition to the cingulate, insula, and the left putamen (*t* score range, −2.59 to −4.68; Cohen's *d* range, −0.89 to −1.60; $P < 0.05$). Conversely, [^{11}C]UCB-J binding was reduced only in 12 subregions including the right middle frontal gyrus, the pre- and postcentral gyri, bilateral superior parietal gyri, posterior temporal, and lateral occipital lobes with large effect sizes (*t* value range, 2.43–4.93; Cohen's *d* range, 0.83–2.15; $P < 0.05$). Widespread cortical and subcortical gray matter volume loss was observed in 46 subregions of the frontal, parietal, temporal, and occipital lobes, as well as the caudate and putamen and thalamus with at least moderate to large affect sizes (*t* value range, 2.47–6.49; Cohen's *d* range, 0.76–2.45; $P < 0.05$) (Table 2A and Supplementary Table S1A, Fig. 2A–left-hand column).

Bayesian Approach. Bayesian statistics corroborate with the results obtained through the frequentist approach above. For differences in [^{18}F]AV-1451 binding between CBS/Aβ+ve and controls, BF_{10} were >3 in 50 regions of interest including frontotemporal–parietal regions, and putamen. For differences in [^{11}C]UCB-J BP_{ND} between CBS/Aβ+ve and controls, BF_{10} was >3 in 44 regions, and >100 in temporal–parietal-occipital regions, cingulate, and subregions of the frontal lobe (precentral gyri and middle frontal gyrus). There was widespread gray matter volume loss, with moderate evidence ($BF_{10} > 3$) in 62 regions in CBS/Aβ+ve (Supplementary Table S3A).

Controls > CBS/Aβ−Ve

Frequentist Approach. Compared to controls, the CBS/Aβ−ve group had increased [^{18}F]AV-1451 binding in three subregions: the left pallidum, right substantia nigra, and the midbrain (*t* value range, −2.45 to −2.82; Cohen's *d* range, −0.71 to −0.84; $P < 0.05$). [^{11}C]UCB-J binding was reduced in nearly all subregions (72/78) across both the cortical mantle and subcortical areas (*t* value range, 2.46–5.69; Cohen's *d* range, 0.74–2.09; $P < 0.05$). Cortical and subcortical gray matter volume loss was observed in 32 subregions including the anterior orbital gyri, middle frontal gyri, parietal lobe subregions, posterior temporal lobe, caudate nucleus, putamen, thalamus, and the cerebellum (*t* value range, 2.42–5.01; Cohen's *d* range, 0.82–1.76; $P < 0.05$) (Table 2B and Supplementary Table S1B, Fig. 2A–middle column).

Bayesian Approach. BF_{10} values were much lower when comparing [^{18}F]AV-1451 binding in CBS/Aβ−ve and controls, with values >3 in the precentral gyri, pallidum, substantia nigra, midbrain, and cerebellar gray matter. Echoing the frequentist results above, there was strong evidence ($BF_{10} > 10$) in support of lower [^{11}C]UCB-J binding in 78 regions with extreme evidence in 67 regions ($BF_{10} > 100$). There was moderate evidence ($BF_{10} > 3$) for widespread gray matter volume loss in 45 regions in the CBS/Aβ−ve, compared to controls (Supplementary Table S3A).

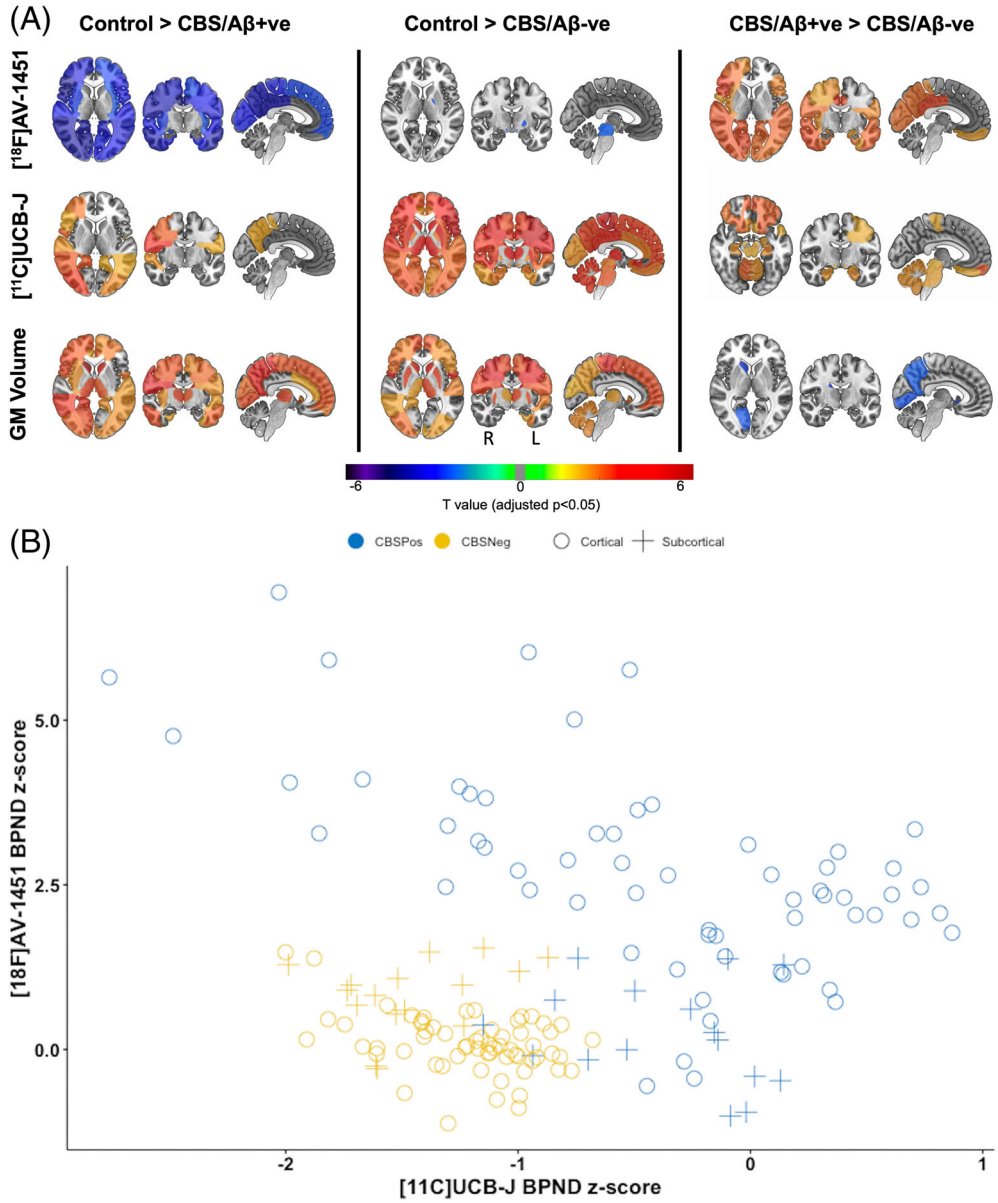

FIG. 2. (**A**) *t*-Statistic brain maps illustrating regional differences in [^{18}F]AV-1451 and [^{11}C]UCB-J non-displaceable binding potential (BP_{ND}) (both partial volume corrected) and gray matter (GM) volume for the following contrasts, controls (Ctrl) > CBS β-amyloid positive (CBS/Aβ+ve) (left-hand column); Ctrl > CBS β-amyloid negative (CBS/Aβ−ve) (middle column); and CBS/Aβ+ve > CBS/Aβ−ve (right-hand column). Only *t* values, significant at $P < 0.05$ corrected for multiple comparisons, are shown here. Higher *t* values for [^{18}F]AV-1451 represent higher binding in CBS/Aβ+ve and CBS/Aβ−ve compared to Ctrl (dark blue) and in CBS/Aβ+ve compared to CBS/Aβ−ve (orange-red). Higher *t* values for [^{11}C]UCB-J regional comparisons, illustrate greater synaptic density in Ctrl versus both patient cohorts and, greater synaptic density in CBS/Aβ+ve versus CBS/Aβ−ve. Higher *t* values for volumetric comparisons show extensive gray matter volume loss in both patient cohorts compared to Ctrl, with more severe loss in CBS/Aβ+ve. (**B**) Scatterplot showing a negative correlation between [^{18}F]AV-1451 and [^{11}C]UCB-J binding (both partial volume corrected) in 78 brain subregions, averaged across CBS/Aβ+ve (blue) and CBS/Aβ−ve (yellow) patients. Values are regional z-scores calculated against Ctrl. Pearson correlation coefficient in CBS/Aβ+ve: $R = -0.49$ ($P < 0.001$), and in CBS/Aβ−ve: $R = -0.36$ ($P = 0.001$). Cortical regions (+), subcortical regions (O).

CBS/Aβ+Ve > CBS/Aβ−Ve

Frequentist Approach. As expected, compared to the CBS/Aβ−ve cohort, the CBS/Aβ+ve group had higher [^{18}F]AV-1451 binding in 48 subregions including all major cortical areas, posterior cingulate, and the cerebellar dentate (*t* value range, 2.50–4.06; Cohen's *d* range, 0.82–1.25; $P < 0.05$). The CBS/Aβ+ve cohort had higher [^{11}C]UCB-J binding in 21 subregions including the orbitofrontal gyri, the precentral gyrus, medial part of the anterior temporal lobe, parahippocampal and hippocampal regions, substantia nigra, pons, and cerebellum (*t* value range, 2.42–3.68; Cohen's *d* range, 0.64–1.35; $P < 0.05$). The differences in [^{11}C]UCB-J binding between CBS/Aβ+ve and CBS/Aβ−ve patients within the frontal lobe, are primarily driven by orbitofrontal subregions (Supplementary

Table S1C)—this may account for the lack of a difference between these two groups when larger aggregate regions are used (eg, frontal lobe), as illustrated in Table 2C. Gray matter volume loss was more pronounced in CBS/Aβ+ve patients in the superior parietal gyrus, anterior temporal lobe, and caudate nucleus (t value range, −2.49 to −3.26; Cohen's d range, −0.92 to −1.56; $P < 0.05$), with the CBS/Aβ−ve showing a lower left substantia nigral volume ($t = 2.63$, Cohen's d 0.85, $P = 0.03$) (Table 2C and Supplementary Table S1C, Fig. 2A–right-hand column).

Bayesian Approach. For differences in [^{18}F]AV-1451 uptake between CBS/Aβ+ve and CBS/Aβ−ve, there was positive evidence for higher cortical binding in CBS/Aβ+ve ($BF_{10} > 3$), and moderate evidence for no difference in brainstem uptake between the two patient cohorts ($BF_{10} < 0.3$). For differences in [^{11}C] UCB-J BP_{ND}, there was anecdotal evidence supporting higher binding in CBS/Aβ+ve in 18 regions, and moderate evidence ($BF_{10} > 3$) in three regions, anterior and lateral orbital gyri and the cerebellar dentate. CBS/Aβ+ve patients had more significant atrophy within the right caudate, medial orbital gyrus, right anterior cingulate, right lingual gyrus, and right anterolateral temporal lobe ($BF_{10} > 3$).

The distinct patterns of [^{18}F]AV-1451 BP_{ND} uptake and synaptic loss ([^{11}C]UCB-J BP_{ND}) in CBS/Aβ+ve and CBS/Aβ−ve cohorts are readily appreciated in the scatterplot in Figure 2B, where at a regional level, patients who are β-amyloid positive have higher [^{18}F] AV-1451 binding and less synaptic loss compared to controls, than those who are β-amyloid negative. In both cohorts, there was a negative relationship between [^{18}F]AV-1451 uptake and [^{11}C]UCB-J BP_{ND} (CBS/Aβ+ve: $R = -0.49$ [$P < 0.001$]; CBS/Aβ−ve: $R = -0.36$ [$P = 0.001$]).

Analyses using partial volume uncorrected data (Supplementary Tables S2A–C and S3B and Supplementary Fig. S2) show slightly more severe synaptic loss in both CBS/Aβ+ve and CBS/Aβ−ve groups compared to controls. However, the distribution of synaptic loss and the differential patterns of loss seen in CBS/Aβ+ve versus CBS/Aβ−ve cohorts remains similar to corrected data, and overall, the results largely echo the findings above, indicating that the differences in synaptic loss are not merely an artefact of atrophy or atrophy correction.

Discussion

There are three main findings of this study. First, the degree and distribution of synaptic loss is clinically correlated in people with CBS, not only in summary rating scales,[26] but also in accord with the laterality of clinical deficits. Second, there is a distinct pattern of synaptic loss, [^{18}F]AV-1451 binding, and gray matter volume loss, in people with CBS according to whether or not they have likely AD as the underlying pathology (ie, are positive or negative for the [^{11}C]PiB amyloid biomarker). Third, synaptic loss is more widespread and more severe in β-amyloid-negative patients with CBS.

Within our cohort, clinical signs were asymmetric in all but one case, in both CBS/Aβ+ve and CBS/Aβ−ve patients. This mirrored the asymmetry of synaptic loss, particularly within the contralateral caudate nucleus, thalamus, cingulate, and ipsilateral cerebellum (Fig. 1 and Supplementary Fig. S1). Laterality on imaging and correlations with asymmetric clinical symptoms have previously been reported for gray matter atrophy, glucose metabolism (as indexed by fludeoxyglucose F18 [[^{18}F]FDG] PET), and [^{18}F]AV1451 binding,[10] and now shown here in terms of asymmetric synaptic loss.

We found distinct patterns of [^{18}F]AV-1451 and [^{11}C]UCB-J binding, and gray matter volume loss in CBS/Aβ+ve versus CBS/Aβ−ve patients, compared to controls. In CBS/Aβ+ve patients who are likely to have AD as the underlying pathology, [^{18}F]AV-1451 binding was diffuse in the cortical gray matter, with particularly high binding in the occipito-parietal lobes and the temporal lobe. Our findings echo reports from previous [^{18}F]AV-1451, and second generation tau PET tracers (eg, [^{18}F]PI-2620),[45] with significant uptake mainly in posterior cortical areas. The extent and degree of gray matter volume loss in our CBS/Aβ+ve cohort, followed that of [^{18}F]AV-1451 binding, but also included subcortical areas. [^{11}C]UCB-J binding potential was mainly reduced in occipito-parietal regions (Supplementary Table S1A and aggregate regions in Table 2A). The pattern of synaptic loss in our CBS/Aβ+ve cohort is similar to that reported in AD by Mecca et al[46] who also reported smaller effect sizes for synaptic loss than for gray matter volume loss.

The CBS/Aβ−ve patients are likely to have corticobasal degeneration as the underlying pathology, although we acknowledge that PSP or frontotemporal lobar degeneration-tau are possible.[1,7,47] We observed a minimal increase in [^{18}F]AV-1451 binding compared to controls, with only the brainstem, and basal ganglia withstanding correction for multiple comparisons. [^{18}F] AV-1451 has a high binding affinity for the paired helical tau filaments in AD, with lower affinity for the straight filaments of 4R tau found in CBD/PSP; its ability to detect non-AD dementias, and to differentiate between the primary tauopathies of CBD and PSP is limited.[39,48] In the CBS/Aβ−ve cohort, gray matter volume loss was extensive, but far less severe than the extent and severity of cortical and subcortical synaptic loss, as shown by significantly reduced [^{11}C]UCB-J BP_{ND} in nearly all subregions in Supplementary Table S1B (and aggregate regions in Table 2B), similar to findings in PSP.[26]

In directly comparing people with CBS/Aβ+ve to those with CBS/Aβ−ve (Table 2C and Supplementary Table S2C), we confirmed higher [^{18}F]AV-1451 uptake across the cortical mantle, with more extensive volumetric loss particularly within the temporal–parietal-occipital subregions and the right caudate in CBS/Aβ+ve patients. Despite this, however, the CBS/Aβ+ve cohort had less severe synaptic loss within both cortical and subcortical areas (Table 2C and Supplementary Table S1C). In other words, the pattern of synaptic loss and tau pathology distinguished CBS/Aβ+ve versus CBS/Aβ−ve cohorts. [^{11}C]UCB-J binding was preferentially reduced in posterior cortical areas in CBS/Aβ+ve patients and more severely lost in anterior cortical and subcortical areas in the CBS/Aβ−ve group. Our results are in line with previous [^{18}F]FDG PET studies in CBS, reporting distinct patterns of glucose hypometabolism in amyloid-positive versus negative CBS and pathologically confirmed CBS-AD, CBS-CBD, and CBS-PSP.[12,13,15,49] [^{18}F]FDG PET is often interpreted as a surrogate of synaptic density. However, our results go further to understand CBS heterogeneity without some of the confounds of [^{18}F]FDG PET (eg, inflammation and functional activation differences)[50] and with the benefit of greater mechanistic specificity of the ligand.

Combining imaging and blood biomarkers in CBS can provide more accurate ante mortem diagnosis of different etiologies, as well as help in understanding the distinct mechanistic pathways leading to a common set of clinical symptoms in this cohort. That the extent of synaptic loss is more severe in CBS/Aβ−ve despite modest gray matter volume loss compared to CBS/Aβ+ve is an interesting finding. It has been shown before in preclinical models[17] and post mortem studies,[27] that synaptic loss can lead ahead of cell death and volume loss and be very closely associated with clinical deficits in tauopathies. Our data do not answer why it is that this difference is more marked in CBS/Aβ−ve cases than CBS/Aβ+ve. We speculate that there is differential synaptotoxicity of 4R tau (likely present in amyloid-negative CBS) than the mixed 3R/4R tauopathy (likely found in CBS-AD).[51] This differential toxicity might also account for the shorter average survival of patients with 4R tauopathies.[52] Another explanation for the differential patterns of synaptic loss could be the likely heterogeneous distribution and progression patterns of tau pathology in CBS-AD versus CBS-CBD/PSP. Although current blood biomarkers such as pTau217 levels or glial fibrillary acidic protein provide high specificity in differentiating between AD and non-AD dementias,[8,53] they do not reveal changes in specific pathological pathways or regions, but rather complement and enrich PET insights.

There are several limitations to this study. First, our sample size is modest, limiting our ability to perform robust classification algorithms for each imaging modality. Despite this, however, we observe moderate/large effect sizes for many of the between and within group comparisons. The Bayesian tests complement the more common frequentists tests, but provide added value in the ability to provide evidence in favor of the null (that there is no group difference), rather than merely a failure to reject the null. Second, in PET studies of neurodegeneration with atrophy, gray matter volume loss can affect the interpretation of PET signals. We used partial volume correction to minimize the effect of atrophy on binding estimates. However, the analyses without partial volume correction yielded similar results in all the main analyses. Third, we used only T1-weighted MRI as a structural marker. Other measures of structural integrity such as diffusion-weighted imaging may provide additional differentiation of the molecular etiologies of CBS.[54] Fourth, we classify our participants according to clinical diagnostic criteria and an arbitrarily thresholded β-amyloid SUVR value. Whereas we interpret that β-amyloid status as indicating likely underlying pathology of AD versus CBD/PSP pathology, this is not confirmed. Other pathologies may also give rise to the CBS,[7,55,56] and co-pathology may also occur that would give rise to a positive β-amyloid scan even in someone with CBD.[57] Last, the cross-sectional design of this study limits the interpretation of the dynamic relationship between pathology and synaptic loss. Although we include patients at various stages and severity of illness, a longitudinal design is necessary to test the dynamic relationship between synaptic loss and gray matter atrophy as disease progresses.

In conclusion, the amyloid status of people with CBS has a marked influence on the severity and distribution of synaptic and gray matter volume loss. Current clinicopathological correlations are poor, with AD causing 30%–50% of CBS and corticobasal degeneration comprising the majority of non-AD etiologies. We do not advocate [^{11}C]UCBJ PET as a diagnostic tool. Rather, it reveals the importance of severe synaptic loss in people with likely CBD, which we hope will inform future therapeutic strategies and improve future clinical trials design. ■

Acknowledgments: We thank the research participants and caregivers, the staff at the Wolfson Brain Imaging Centre, and at the Cambridge Centre for Parkinson-Plus. We thank UCB Pharma, and Avid, for providing the precursor for [^{11}C]UCB-J, and [^{18}F]AV-1451, respectively.

Data Availability Statement

Anonymised derived data at subject- region- and modality-level that support the findings of this study are available from the corresponding author without restriction. Clinical and raw imaging data may be

requested, but are subject to restrictions and likely need for a material transfer agreement to preserve participant confidentiality.

References

1. Koga S, Josephs KA, Aiba I, Yoshida M, Dickson DW. Neuropathology and emerging biomarkers in corticobasal syndrome. J Neurol Neurosurg Psychiatry 2022;93(9):919–929.
2. Armstrong MJ, Litvan I, Lang AE, et al. Criteria for the diagnosis of corticobasal degeneration. Neurology 2013;80:496–503.
3. Burrell JR, Hodges JR, Rowe JB. Cognition in corticobasal syndrome and progressive supranuclear palsy: a review. Mov Disord 2014;29(5):684–693.
4. Boeve BF, Lang AE, Litvan I. Corticobasal degeneration and its relationship to progressive supranuclear palsy and frontotemporal dementia. Ann Neurol 2003;54(S5):S15–S19.
5. Mathew R, Bak TH, Hodges JR. Diagnostic criteria for corticobasal syndrome: a comparative study. J Neurol Neurosurg Psychiatry 2012;83(4):405–410.
6. Höglinger GU, Respondek G, Stamelou M, et al. Clinical diagnosis of progressive supranuclear palsy: the movement disorder society criteria. Mov Disord 2017;32:853–864.
7. Alexander SK, Rittman T, Xuereb JH, Bak TH, Hodges JR, Rowe JB. Validation of the new consensus criteria for the diagnosis of corticobasal degeneration. J Neurol Neurosurg Psychiatry 2014; 85:923–927.
8. Zetterberg H, Schott JM. Blood biomarkers for Alzheimer's disease and related disorders. Acta Neurol Scand 2022;146(1):51–55.
9. Toledo JB, Zetterberg H, van Harten AC, et al. Alzheimer's disease cerebrospinal fluid biomarker in cognitively normal subjects. Brain 2015;138(Pt 9):2701–2715.
10. Wilson H, de Natale ER, Politis M, Niccolini F. Chapter 14-neuroimaging in corticobasal syndrome. In: Politis M, Wilson H, de Natale ER, eds. Neuroimaging in Parkinson's Disease and Related Disorders. Cambridge: Academic Press; 2023:399–417.
11. Sha SJ, Ghosh PM, Lee SE, et al. Predicting amyloid status in corticobasal syndrome using modified clinical criteria, magnetic resonance imaging and fluorodeoxyglucose positron emission tomography. Alzheimers Res Therapy 2015;7(1):8.
12. Pardini M, Huey ED, Spina S, et al. FDG-PET patterns associated with underlying pathology in corticobasal syndrome. Neurology 2019;92(10):e1121–e1135.
13. Benvenutto A, Guedj E, Felician O, et al. Clinical phenotypes in Corticobasal syndrome with or without amyloidosis biomarkers. J Alzheimers Dis 2020;74(1):331–343.
14. Parmera JB, Coutinho AM, Neto AS, et al. Degeneration patterns on [18F]FDG-PET predict amyloid deposition in corticobasal syndrome. Alzheimers Dement 2020;16(S5):e041878.
15. Parmera JB, Coutinho AM, Aranha MR, et al. FDG-PET patterns predict amyloid deposition and clinical profile in Corticobasal syndrome. Mov Disord 2021;36(3):651–661.
16. Whitwell JL, Josephs KA. Neuroimaging in frontotemporal lobar degeneration-predicting molecular pathology. Nat Rev Neurol 2012; 8:131–142.
17. Kaniyappan S, Chandupatla RR, Mandelkow EM, Mandelkow E. Extracellular low-n oligomers of tau cause selective synaptotoxicity without affecting cell viability. Alzheimers Dement 2017;13:1270–1291.
18. Finnema SJ, Nabulsi NB, Eid T, et al. Imaging synaptic density in the living human brain. Sci Transl Med 2016;8:348ra96.
19. Chen MK, Mecca AP, Naganawa M, et al. Assessing synaptic density in Alzheimer disease with synaptic vesicle glycoprotein 2A positron emission tomographic. Arch Neurol 2018;75:1215–1224.
20. Mecca AP, Chen MK, O'Dell RS, et al. In vivo measurement of widespread synaptic loss in Alzheimer's disease with SV2A PET. Alzheimers Dement 2020;16:alz.12097.
21. Malpetti M, Holland N, Jones PS, et al. Synaptic density in carriers of C9orf72 mutations: a [(11) C]UCB-J PET study. Ann Clin Transl Neurol 2021;8:1515–1523.
22. Malpetti M, Jones PS, Cope TE, et al. Synaptic loss in frontotemporal dementia revealed by [(11) C]UCB-J PET. Ann Neurol 2022;93:142–154.
23. Andersen KB, Hansen AK, Damholdt MF, et al. Reduced synaptic density in patients with Lewy body dementia: an [(11) C]UCB-J PET imaging study. Mov Disord 2021;36(9):2057–2065.
24. Andersen KB, Hansen AK, Schacht AC, et al. Synaptic density and glucose consumption in patients with Lewy body diseases: an [(11) C]UCB-J and [(18) F]FDG PET study. Mov Disord 2023; 38(5):796–805.
25. Matuskey D, Tinaz S, Wilcox KC, et al. Synaptic changes in parkinson disease assessed with in vivo imaging. Ann Neurol 2020; 87:329–338.
26. Holland N, Jones PS, Savulich G, et al. Synaptic loss in primary Tauopathies revealed by [(11) C]UCB-J positron emission tomography. Mov Disord 2020;35(10):1834–1842.
27. Terry RD, Masliah E, Salmon DP, et al. Physical basis of cognitive alterations in alzheimer's disease: synapse loss is the major correlate of cognitive impairment. Ann Neurol 1991;30:572–580.
28. Holland N, Jones PS, Savulich G, et al. Longitudinal synaptic loss in primary Tauopathies: an in vivo [(11) C]UCB-J positron emission tomography study. Mov Disord 2023;38(7):1316–1326.
29. Golbe LI, Ohman-Strickland PA. A Clinical Rating Scale for Progressive Supranuclear Palsy. Brain: Oxford University Press; 2007: 1552–1565.
30. Lang AE, Stebbins GT, Wang P, et al. The Cortical Basal ganglia Functional Scale (CBFS): Development and preliminary validation. Parkinsonism Relat Disord 2020;79:121–126. doi:10.1016/j.parkreldis.2020.08.021
31. Burgos N, Cardoso MJ, Thielemans K, et al. Attenuation correction synthesis for hybrid PET-MR scanners: application to brain studies. IEEE Trans. Med. Imaging 2014;33:2332–2341.
32. Avants BB, Epstein CL, Grossman M, Gee JC. Symmetric diffeomorphic image registration with cross-correlation: evaluating automated labeling of elderly and neurodegenerative brain. Medical Image Analysis 2008;12:26–41.
33. Meltzer CC, Leal JP, Mayberg HS, Wagner HN Jr, Frost JJ. Correction of PET data for partial volume effects in human cerebral cortex by MR imaging. J Comput Assist Tomogr 1990;14(4):561–570.
34. Wu Y, Carson RE. Noise reduction in the simplified reference tissue model for neuroreceptor functional imaging. J Cereb Blood Flow Metab 2002;22(12):1440–1452.
35. Koole M, van Aalst J, Devrome M, et al. Quantifying SV2A density and drug occupancy in the human brain using [11 C]UCB-J PET imaging and subcortical white matter as reference tissue. Eur J Nucl Med Mol Imaging 2019;46:396–406.
36. Rossano S, Toyonaga T, Finnema SJ, et al. Assessment of a white matter reference region for (11)C-UCB-J PET quantification. J Cereb Blood Flow Metab 2020;40(9):1890–1901.
37. Gunn RN, Lammertsma AA, Hume SP, Cunningham VJ. Parametric Imaging of Ligand-Receptor Binding in PET Using a Simplified Reference Region Model. NeuroImage: Academic Press; 1997:279–287.
38. Jack CR Jr, Wiste HJ, Schwarz CG, et al. Longitudinal tau PET in ageing and Alzheimer's disease. Brain 2018;141(5):1517–1528.
39. Leuzy A, Chiotis K, Lemoine L, et al. Tau PET imaging in neurodegenerative tauopathies-still a challenge. Mol Psychiatry 2019;24(8): 1112–1134.
40. Klunk WE, Koeppe RA, Price JC, et al. The Centiloid project: standardizing quantitative amyloid plaque estimation by PET. Alzheimers Dement 2015;11:1–15.e14.
41. Jack CR, Wiste HJ, Weigand SD, et al. Age-specific and sex-specific prevalence of cerebral β-amyloidosis, tauopathy, and neurodegeneration in cognitively unimpaired individuals aged 50–95 years: a cross-sectional study. Lancet Neurol 2017;16:435–444.
42. Ito KL, Liew S-L. Calculating the laterality index using FSL for stroke neuroimaging data. GigaScience 2016;5(suppl_1): s13742-016-0147-0-n.

43. Team J. JASP. 0.16.2 Ed. Amsterdam, Netherlands: JASP Foundation; 2022.
44. Kass RE, Raftery AE. Bayes factors. J Am Stat Assoc 1995;90(430): 773–795.
45. Blazhenets G, Soleimani-Meigooni DN, Thomas W, et al. [(18)F]PI-2620 binding patterns in patients with suspected Alzheimer disease and frontotemporal lobar degeneration. J Nucl Med 2023;64(12): 1980–1989.
46. Mecca AP, Chen MK, O'Dell RS, et al. Alzheimer's & Dementia. Alzheimers Dement 2020;16:974.
47. Rösler TW, Tayaranian Marvian A, Brendel M, et al. Four-repeat tauopathies. Prog Neurobiol 2019;180:101644.
48. Ono M, Sahara N, Kumata K, et al. Distinct binding of PET ligands PBB3 and AV-1451 to tau fibril strains in neurodegenerative tauopathies. Brain 2017;140(3):764–780.
49. Cerami C, Dodich A, Iannaccone S, et al. Individual brain metabolic signatures in Corticobasal syndrome. J Alzheimers Dis 2020;76(2): 517–528.
50. Rahman WT, Wale DJ, Viglianti BL, et al. The impact of infection and inflammation in oncologic (18)F-FDG PET/CT imaging. Biomed Pharmacother 2019;117:109168.
51. Vourkou E, Paspaliaris V, Bourouliti A, et al. Differential effects of human tau isoforms to neuronal dysfunction and toxicity in the drosophila CNS. Int J Mol Sci 2022;23(21):12985.
52. Jabbari E, Holland N, Chelban V, et al. Diagnosis across the Spectrum of progressive Supranuclear palsy and Corticobasal syndrome. JAMA Neurol 2020;77(3):377–387.
53. VandeVrede L, La Joie R, Thijssen EH, et al. Evaluation of plasma phosphorylated Tau217 for differentiation between Alzheimer disease and frontotemporal lobar degeneration subtypes among patients with Corticobasal syndrome. JAMA Neurol 2023;80(5): 495–505.
54. Correia MM, Rittman T, Barnes CL, Coyle-Gilchrist IT, Ghosh B, Hughes LE, Rowe JB. Towards accurate and unbiased imaging-based differentiation of Parkinson's disease, progressive supranuclear palsy and corticobasal syndrome. Brain Commun 2020;2: fcaa051.
55. Respondek G, Kurz C, Arzberger T, et al. Which ante mortem clinical features predict progressive supranuclear palsy pathology? Mov Disord 2017;32:995–1005.
56. Respondek G, Grimm MJ, Piot I, et al. Validation of the movement disorder society criteria for the diagnosis of 4-repeat tauopathies. Mov Disord 2020;35(1):171–176. doi:10.1002/mds.27872
57. Mizutani Y, Ohdake R, Tatebe H, et al. Associations of Alzheimer's-related plasma biomarkers with cognitive decline in Parkinson's disease. J Neurol 2023;270(11):5461–5474.

Supporting Data

Additional Supporting Information may be found in the online version of this article at the publisher's web-site.

SGML and CITI Use Only
DO NOT PRINT

Author Roles

(1) Research project: A. Conception, B. Organization, C. Execution; (2) Statistical Analysis: A. Design, B. Execution, C. Review and Critique; (3) Manuscript: A. Writing of the First Draft, B. Review and Critique.

N.H., J.T.O., J.B.R.: 1A, 2A
N.H.: 1A, 1B, 1C, 2A, 2B, 2C, 3A, 3B
P.S.J., G.S., M.N., M.M., D.J.W., D.S., P.S., E.M., T.D.F., Y.T.H., T.R.: 2B, 2C, 3B
F.I.A., K.B.: 2B, 3B
J.T.O., J.B.R.: 1A, 1B, 2A, 2C, 3B

Financial Disclosures of all Authors (for the Preceding 12 Months)

In the last 12 months the authors were supported by the Wellcome Trust (220258), Cambridge Centre for Parkinson-Plus (RG95450); the National Institute for Health and Care Research (NIHR) Cambridge Biomedical Research Centre (NIHR203312); Medical Research Council (MC_UU_00030/14; MR/T033371/1); and Race Against Dementia Alzheimer's Research United Kingdom (ARUK-RADF2021A-010).